Hindawi
Shock and Vibration
Volume 2021, Article ID 5559260, 17 pages
https://doi.org/10.1155/2021/5559260

Research Article

Seismic Fragility Assessment of RC Plan-Asymmetric Wall-Frame Structures Based on the Enhanced Damage Model

Ning Wang,[1] **Xiaoning Huang**,[2] **and Dan Zhang**[2]

[1]*School of Civil Engineering, Lanzhou University of Technology, Lanzhou, Gansu 730050, China*
[2]*Qinghai Provincial Key Laboratory of Energy-Saving Building Materials and Engineering Safety, Civil Engineering College, Qinghai University, Xining, Qinghai 810016, China*

Correspondence should be addressed to Xiaoning Huang; hxiaoning7191@163.com

Received 4 February 2021; Revised 18 September 2021; Accepted 21 September 2021; Published 1 November 2021

Academic Editor: Ricardo A. Ramirez-Mendoza

The seismic response of reinforced concrete (RC) plan-asymmetric structures is significantly influenced by the input angle of seismic ground motions. Hence, it is challenging to assess the performance of plan-asymmetric structures. In this study, the classic probabilistic seismic fragility assessment method is used to assess RC plan-asymmetric wall-frame structures based on the enhanced damage model. First, the worst-case input angle of seismic ground motions for plan-asymmetric structures is identified using the wavelet transforms coefficient method, considering the coupling of bidirectional seismic ground motions. Accordingly, the maximum deformation and hysteretic energy dissipation can be determined. Then, an enhanced damage model, which is based on the combination of deformation and hysteretic energy dissipation, is used to identify floor damage factor. Note that the importance coefficients of structural components are considered in the identification. Meanwhile, the incremental dynamic analysis (IDA) is conducted to create the fragility curves by assuming floor damage factor as seismic performance index. In particular, the randomness of the threshold for floor damage factor is considered during the assessment. Afterwards, numerical simulations are employed to verify the fragility assessment method. Results show that the wavelet transforms coefficient method can evaluate the worst-case input angles with low time-consuming and high efficiency. Meanwhile, the story damage factors confirmed that the proposed damage model could accurately assess the structure during the failure process. Moreover, the typical failure modes of the RC wall-frame structure, which significantly depend on the story damage distribution, can be defined using the enhanced damage model. Note that the randomness of the threshold could significantly affect the probability of exceedance, which is important for fragility analysis.

1. Introduction

The seismic records are time-domain signals that can represent the total input energy of seismic ground motions. For a certain seismic record, the total energy input is the same; if the input angle is different, the dynamic response is different even for the same structure [1]. The conventional seismic performance evaluation of structures generally assumes that the input angle of seismic ground motion is along the main axis of structure, ignoring the uncertainty of the input angle, which may overestimate the seismic performance of structure [2]. Studies have shown that the input angle of seismic ground motion impacts more the seismic performance evaluation results of plan-asymmetric structures than that of plan-symmetric structures. Zhu et al. [3, 4] investigated the principle input angle of irregular bridges based on the square root of the sum of the squares (SRSS) combination method and reported that the maximum response of an irregular bridge could be obtained using the response spectrum analysis input along two arbitrary in-plane directions. Factors such as the curvature and connection type of the pier and beam were also analyzed. Ni [5] investigated the influence of the seismic ground motions input angle on the seismic response of a curved girder bridge. Therefore, it

is very important to determine the worst-case input angle of seismic ground motion, which is one of the main methods to analyze the impact of the input angle of seismic ground motion on the seismic performance evaluation results of plan-asymmetric structures.

When the input angle of seismic ground motion changes, for the structures, the frequency domain of seismic ground motion also changes, so we can analyze the impact on structural responses induced by input angle through obtaining the frequency domain of seismic ground motion [6, 7]. Conventionally, the overall frequency domain information of seismic ground motion is obtained through Fourier transform or power spectrum analysis. In these types of methods, nonstationary characteristics of seismic ground motions are not taken into account; given this, researchers put forward the concept of "windowing" and developed it into a short-time Fourier transform, by which nonstationary characteristics are considered. However, because "windowing" is constant, it cannot solve the contradiction between calculation accuracy and calculation amount. Based on this, researchers have introduced the "changing window" method, which is the wavelet transform used now [8]. Time process of different frequency components signals of the seismic ground motion can be obtained through the continuous wavelet transform of the seismic signal. Also, nonstationarity of the seismic ground motion can be considered through the continuous wavelet transform, which makes the frequency domain of the seismic ground motion more realistic [8, 9]. In this article, continuous wavelet transform was used to acquire the frequency domain of seismic ground motions with different input angles, by which the worst-case input angle was obtained. Then, seismic performance evaluation of structure under the seismic ground motion with the worst-case input angle is conducted, and the safety reserve of the structure is improved.

RC wall-frame structures have been widely used in practical engineering for their excellent seismic performance. The seismic performance evaluation method based on reliability theory has always been an issue of interest for engineers around the world and can be used for various purposes in the field of earthquake resistance. Fragility assessment is a key part of seismic reliability analysis. Presently, fragility analysis is an effective technique for the probabilistic assessment of seismic risk, which can help structural designers in developing performance-based seismic design during the decision-making process [10, 11]. Many studies have been conducted to develop fragility curves for structures under earthquake excitation [12, 13]. Tajammolian et al. [14] carried out sensitivity analysis for the fragility curves derived for different RC frames under two site classes and amplification functions in the Erzincan region. Bhandari et al. [15] conducted fragility analysis for the probabilistic seismic risk assessment of a base-isolated frame building under near- and far-field earthquakes. The seismic performance evaluation methods aforementioned are mostly based on displacement. However, it has been found through seismic damage investigations and theoretical research that there are two main causes for the damage of RC wall-frame structure [16]. (1) Because of the excessive hysteretic energy dissipation, oblique cracks appear in the shear-wall limbs at the bottom of the structure and concrete at the root of the shear-wall is cracked. (2) Due to the excessive deformation, coupling beams and frame beams on the upper floors are damaged. When a structure encounters an earthquake, it will deform and experience the process of energy dissipation. Both deformation and energy dissipation can cause damage to the structure, and the structure will fail or even collapse after the damage reaching a certain level. As a result, the degree of structural damage may be underestimated, if displacement is the only index to evaluate the seismic performance of the structure. Recently, numerous damage models have been developed, aiming to describe the damage evolution law and define the damage states caused by earthquake excitation for components and structures [17–19]. Park et al. [20, 21] proposed a dual-parameter element damage model based on deformation and energy dissipation and also proposed a floor damage model based on energy dissipation ratio. Du and Ou [22] considered that the more severely damaged components have the greater impact on floor damage and proposed a story damage model based on damage ratio. In these damage models, different components with equal damage have the same impact on the story damage. But from the perspective of practical engineering design, for RC wall-frame structure, beams, especially coupling beams, are expected to consume part of the seismic action through its plastic deformation. Therefore, when the shear-wall and the beam are equally damaged, the shear-wall has significantly greater damage to the whole story damage than that of the beam. In this study, the importance coefficient of component is introduced into the story damage model based on the damage ratio, by which we can consider how the degree of the story damage is affected by different kinds of components.

A novel method is proposed to identify the worst-case input angle for structures using the wavelet transforms coefficient method. An enhanced damage model, in which the importance coefficients of structural components are taken into account, is presented to identify story damage factor based on the combination of deformation and hysteretic energy dissipation. Then, a numerical analysis model of a plan-asymmetric RC wall-frame structure is established using Perform-3D (a finite element analysis software), and 20 seismic ground motions are selected according to the seismic ground motion recommended by Chinese code for seismic design of buildings [23]. Each of the selected seismic ground motions is used to obtain the damage factors of the structure under the worst-case input angle of itself, and the incremental analysis (IDA) is conducted to generate the fragility curves. Particularly, the randomness of the threshold is considered during the assessment. Finally, numerical simulations are employed to verify the enhanced method.

2. Determination of the Worst-Case Input Angle of Seismic Ground Motions

2.1. The Wavelet Transforms. The continuous wavelet transform is written as

$$C(a,b) = \int_{-\infty}^{\infty} f(t)\varphi(a,b,t)\mathrm{d}t, \quad (1)$$

where $\varphi(a, b, t)$ is a wavelet function, and $C(a, b)$ is a wavelet transform coefficient associated with scale coefficient, a, and position coefficient, b.

With the wavelet transforms of seismic ground motion, different wavelet transform variation coefficients $C(a,$ b) can be obtained, and the corresponding wavelet energy distribution is

$$E(a,b) = |C(a,b)|^2. \quad (2)$$

According to Equation (2), the concept of effective input energy is introduced to calculate the wavelet energy distribution of different wavelet transform variation coefficients intuitively and concisely, which is defined as the area enclosed by $C(a, b)$ and the time axis. $C(a, b)$ is a function of the scale coefficient a and the position coefficient b. When a is constant, the wavelet function moves along the time axis on the signal by changing b, and the effective input energy corresponding to $C(a, b)$ does not change. While a is variable, the frequency range of $C(a, b)$ changes, and the frequency component of the signal in the frequency center also changes; as a result, the effective input energy changes, as shown in Figure 1.

Comparing figures (1-b) and (1-c), it can be observed that, with the change of a, $C(a, b)$ as well as the area enclosed by $C(a, b)$ and the time axis all change significantly. Therefore, the parameter that affects the effective input energy corresponding to $C(a, b)$ is a, and the effective input energy of the signal can be obtained by determining a.

Based on the wavelet transform, the signal $f(t)$ is transformed into the wavelet transforms coefficient $C(a, b)$. The relationship between the center frequency of the wavelet, F_c, and the frequency of the structure, F_a, can be written as Equation (3). The 4th order Daubechies ('db4') wavelet function, which is close to the characteristics of seismic records, is selected in the article. The schematic diagram of the 'db4' wavelet function is shown in Figure 2, in which F_c equals 0.7143 Hz.

$$F_a = \frac{F_c}{\Delta \times a}, \quad (3)$$

where Δ is the sampling interval. The scale coefficient, a, can be obtained according to the frequency of the structure using Equation (3). Hence, the worst-case input angle can be obtained for a single-degree-of-freedom system using the wavelet transforms coefficient method. However, structures, especially the plan-asymmetric structures, are direction-sensitive. The structural responses change significantly with the variation of ground motion directions. It is meaningful to obtain the worst-case input angle for the structure with multiple frequencies using the wavelet transforms coefficient method.

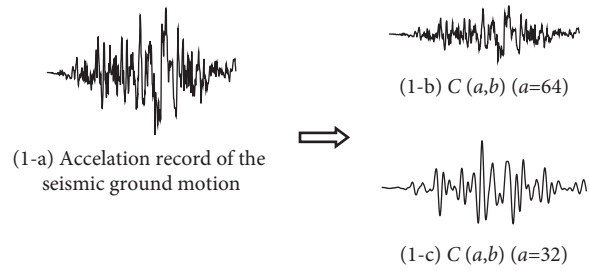

Figure 1: Schematic diagram of $C(a, b)$ of seismic ground motion.

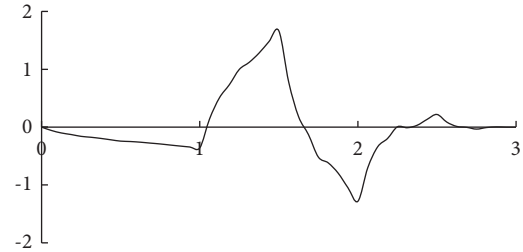

Figure 2: Schematic diagram of 'db4' wavelet.

2.2. The Worst-Case Input Angle of Seismic Ground Motions. The value of structural response significantly increases, when the frequency of earthquake increases to the structural fundamental frequency [9]. The wavelet transforms coefficient method, which can decompose the ground motions into different frequency components, can be used to obtain the energy of different frequency components. In this article, the method for determining the worst-case input angle of bidimensional seismic ground motion through wavelet transforms coefficient method is proposed, which is suitable for both plan-asymmetric and plan-symmetric structures, and a plan-asymmetric structure is taken as an example, as shown in Figure 3. The method is presented in the following steps:

Step 1: The initial input angles of the bidimensional seismic ground motions are along the orthogonal coordinate axes, X_θ and Y_θ, respectively. According to the orthogonal decomposition, the seismic ground motion is transferred into two new components, which are orthogonal, $\ddot{x}_g$ and $\ddot{y}_g$, i.e. $\ddot{x}_g = X_\theta \cos\theta + Y_\theta \sin\theta$, $\ddot{y}_g = Y_\theta \cos\theta - X_\theta \sin\theta$, and θ is the angle between the axis X_θ and axis $\ddot{x}_g$, which varies from 0° to 180° by step 20°, as shown in Figure 3.

Step 2: Based on Equation (3), the scale parameters, a, for different modes of the structure can be calculated according to the center frequency of the wavelet and corresponding model frequency of the structure. Accordingly, the new components are decomposed into different frequency components using the wavelet transforms with the obtained scale parameters. Hence, the wavelet coefficient curve is obtained, and the area

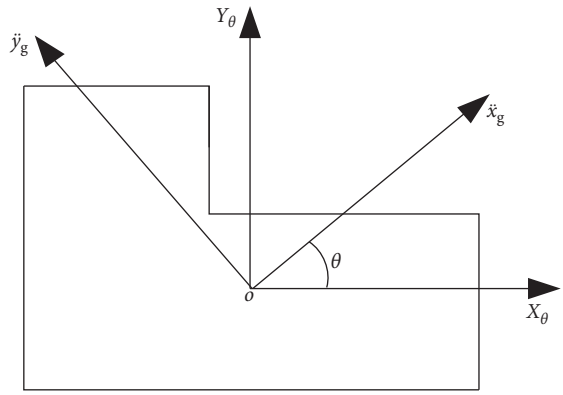

Figure 3: The input angle of a plan-asymmetric structure.

below the curve represents the effective input energy of the ground motion.

Step 3: The effective input energy corresponding to the input angle, θ, is determined as the maximum of the effective input energy for the considered modes. Moreover, the value of structural responses increases with the increase of effective input energy. Hence, the angle corresponding to the maximum effective input energy is the worst-case input angle of the seismic ground motion for considered structure.

3. The Enhanced Damage Model for RC Structures

3.1. Method for Calculating the Damage Factor of the Structural Component. The dual-parameters damage model is the most widely used damage model at present, which is combined with maximum deformation and energy dissipation. Among those dual-parameter damage models, the most representative one is the dual-parameters seismic damage model proposed by Park and Alfredo Ang [21], which is based on experimental data from the destruction test of RC components, and deformation and accumulated hysteretic energy are considered in this model, as shown in Equations (4)–(6).

$$D_{if} = D_{\text{bif}} + D_{\text{hif}}, \tag{4}$$

$$D_{\text{bif}} = \frac{\delta_m}{\delta_u}, \tag{5}$$

$$D_{\text{hif}} = \beta \frac{\int d\varepsilon}{Q_y \delta_u}, \tag{6}$$

where D_{if} is the damage factor of component i on the f^{th} story; D_{bif} is the damage factor of component i caused by deformation of the f^{th} story; D_{hif} is the damage factor of component i caused by energy dissipation of the f^{th} floor; δ_m is the maximum displacement of component under earthquake action; δ_m is the ultimate displacement of component under monotonic load; Q_y is the yield strength of the component; $\int d\varepsilon$ is the total hysteretic energy dissipation of the component; β is the system combination parameter, as shown in

$$\beta = \left(-0.447 + 0.073\lambda + 0.24\lambda_N + 0.314\rho\right)^* 0.7\rho_w. \tag{7}$$

In Equation (7), λ is the shear span ratio, when $\lambda < 1.7$, $\lambda = 1.7$ is taken; λ_N is the axial compression ratio, when $\lambda_N < 0.2$, $\lambda_N = 0.2$ is taken; ρ is the longitudinal reinforcement ratio; ρ_ω is the volumetric stirrup ratio, when $\rho_\omega > 2\%$, $\rho_\omega = 2\%$ is taken; generally, the value range of β is 0~0.85.

3.2. The Classical Damage Model for RC Structures. The component damage model used in this paper is proposed by Park-Ang, which has been tested and verified in Reference [20]. Generally, the global structural damage model can be regarded as a combination of element damage models. Once damage factors of components are determined, the damage factor of global model can be obtained by combining weighted damage factors of components. Park-Ang proposed a story damage model in Reference [21] and defined the weighted combination coefficient as the ratio of the energy consumption of each component in a certain story and that of the global story, as shown in Equations (8) and (9):

$$D_f = \sum_{i=1}^{n} \lambda_{\text{if}} D_{\text{if}}, \tag{8}$$

$$\lambda_{\text{if}} = \frac{E_{\text{if}}}{\sum_{i=1}^{n} E_{\text{if}}}, \tag{9}$$

where D_f is the damage factor of the f^{th} story; λ_{if} is the weighted combination coefficient of component i in the f^{th} stoty; E_{if} is the hysteretic energy dissipation of component i in the fth story.

Based on the story damage model proposed by Park-Ang, Du and Ou [22] considered that the more severely damaged elements have a greater impact on the story damage, so the damage factor of the component is taken as the weighting coefficient:

$$\lambda_{\text{if}} = \frac{D_{\text{if}}}{\sum_{i=1}^{n} D_{\text{if}}}. \tag{10}$$

However, component importance was not considered in the story damage model proposed by Park et al. [20] and Du and Ou [22], which means that, in these models, the importance of components is not distinguished when the weighted combination coefficient is valued. As a matter of fact, the more important the component is, the larger the weighted combination coefficient value should be. Especially, for RC wall-frame structures, if the component importance is not considered, when the coupling beams and shear-walls on the same story were equally damaged, the coupling beams and shear-walls have the same effect on the whole story damage. Studies have shown that, under the strong seismic ground motions, the coupling beams and frame beams are damaged first, but a certain degree of damage has little effect on the global performance of the structure. When the earthquake action becomes stronger, the shear-walls are damaged. Even though the shear-walls are slightly damaged, the global performance of the structure

may be obviously degraded. Therefore, it is necessary to distinguish the importance of different components by modifying the weighted combination coefficients. The basic principle for determining the weighted combination coefficient is to reflect the relative importance of each component in maintaining the global stability of the structure. Key components that may induce the collapse of the structure should be given a larger weighted combination coefficient. In general, the influence of the component importance coefficient should be considered in the weighted combination coefficient of the global damage model.

3.3. The Importance Coefficient of Structural Component. The importance coefficient refers to the influence of structural component failure on the strain energy of structures, which is significantly influenced by the mechanical property and load form of structures. Recently, the load-related evaluation method has been proposed for the determination of the importance coefficient, in which the transfer path of loads is considered in Reference [24]. The strain energy of the initial structure is

$$U = \frac{1}{2}\{F\}^T\{D\}, \tag{11}$$

where $\{F\}^T$ is the load vector of the structure, $\{D\}$ is the displacement vector of the structure, and U is the strain energy of the initial structure.

The structural displacement vector is equivalent to the generalized displacement, D_S, under the generalized force F_S. Accordingly, the corresponding generalized stiffness of the structure can be calculated using

$$K_S = \frac{F_S}{D_S}. \tag{12}$$

Hence, the strain energy of the structure can be calculated using

$$U = \frac{1}{2}F_S^2\frac{1}{K_S}. \tag{13}$$

Inversely, the generalized stiffness can be calculated based on the strain energy, U, and the generalized force, F_S

$$K_S = \frac{1}{2}F_S^2\frac{1}{U}. \tag{14}$$

According to Equation (14), the generalized stiffness of the structure is related to the load and strain energy of the structure. The importance coefficient can be defined as the loss rate of the generalized stiffness resulted by component failure:

$$I_i = \frac{K_{N,0} - K_{N,i}}{K_{N,0}}, \tag{15}$$

where I_i is the loss rate of the generalized stiffness, which represents the importance coefficient; $K_{N,0}$ and $K_{N,i}$ are the generalized stiffness of the initial structure and the residual structure after the failure of component i, respectively. The range of I_i is from 0 to 1. The component i does not affect the generalized stiffness of the structure, when $I_i = 0$, whereas the generalized stiffness is fully dependent on component i, when $I_i = 1$. The importance coefficient is closely related to the importance of the structural component.

3.4. The Enhanced Damage Model for RC Structures. The story damage of structure is significantly impacted by component importance. However, the conventional story damage models are mainly based on the deformation and hysteretic energy dissipation of structural component [20, 22, 25–28], in which the component importance is ignored. It is meaningful to enhance the traditional damage model by distinguishing the importance of different structural components (i.e., column, frame beam, coupling beam, and shear-wall). Hence, II damage model, in which the component importance is considered, is proposed. Structural components are assigned with different weight coefficients in the II damage model. The weight coefficient is calculated according to the importance coefficient, deformation, and hysteretic energy dissipation of structural components.

The story damage factor of f^{th} story, which consists of n structural components, can be calculated using Equations (16)–(20):

$$\lambda_{\text{bif}} = \frac{I_{\text{if}}D_{\text{bif}}}{\sum_{i=1}^{\text{n}} I_{\text{if}}D_{\text{bif}}}, \tag{16}$$

$$\lambda_{\text{bif}} = \frac{I_{\text{if}}D_{\text{hif}}}{\sum_{i=1}^{\text{n}} I_{\text{if}}D_{\text{hif}}}, \tag{17}$$

$$D_f = D_{bf} + D_{hf}, \tag{18}$$

$$D_{bf} = \sum_{i=1}^{n} \lambda_{\text{bif}}D_{\text{bif}}, \tag{19}$$

$$D_{hf} = \sum_{i=1}^{n} \lambda_{\text{hif}}D_{\text{hif}}, \tag{20}$$

where D_{bf} and D_{hf} are the damage factors of f^{th} story caused by the deformation and hysteretic energy dissipation, respectively; λ_{bif} and λ_{hif} are weighted combination coefficients of component i on f^{th} story corresponding to deformation and hysteretic energy dissipation, respectively; and I_{if} is the importance coefficient of component i on f^{th} story, which can be obtained according to Section 3.3; D_{bif} and D_{hif} can be obtained by Equations (5) and (6).

3.5. The Threshold of Damage Factor. The threshold of damage factor for different performance levels is shown in Table 1. The damage model proposed in this article can be used to assess the damage incurred by columns, frame beams, coupling beams, shear-walls, and so on, which are vital structural components. However, it is necessary to define failure criteria to identify the damage states of components during the loading process. Therefore, RC structures damaged under earthquake excitation are used to validate the proposed

damage evaluation method, and practical structural damage limits are defined accordingly. Damage factor can be used to quantify costs and other consequences related to the damage of structures or components, for example, potential risks after an earthquake. According to damage states, a damage factor value equal to 0 generally indicates no damage, a value of 0.1 indicates slight damage, a damage value of 0.3 indicates moderate damage, and a damage value of 0.6 indicates severe damage. Components and structures with values of damage factors greater than 0.85 are considered to be approaching collapse [29], as shown in Table 1, 'NO' represents the structures without damage, 'IO' represents the structures with small damage and those that have been yielded, 'LS' represents the structures with severe damage, and 'CP' represents the structures approaching collapse.

4. Seismic Fragility Assessment Method

The seismic fragility is defined as the probability of exceeding the defined damage state or threshold of a component or structure for a specific earthquake intensity and can generally be modeled by a lognormal probability distribution function [30, 31]:

$$\begin{aligned} F &= P\left\{\left(D \geq D_{LS_i} | I\right)\right\} \\ &= P\left\{\left(\frac{D}{D_{LS_i}} \geq 1\right) | I\right)\right\}, \end{aligned} \tag{21}$$

where D is the maximum story damage factor, which can be calculated using Equations (8)–(12), and D_{LS_i} is the threshold for story damage factor of the ith performance level, as shown in Table 1.

Generally, the response of the story damage factor is random variables, which is approximated by a lognormal distribution, the threshold of the story damage factor is constant, and the probability of exceedance, P_f, can be expressed by

$$P_f = \Phi\left(\frac{\ln\left(\mu_D\right) - \ln\left(D_{LS_i}\right)}{\sigma_{\ln D}}\right), \tag{22}$$

where $\Phi(\cdot)$ is the standard normal probability distribution, μ_D is the mean value of the maximum story damage factor, and $\sigma_{\ln D}$ is the standard deviation of the maximum story damage factor.

The response and threshold of the story damage factor are both random variables modeled by the lognormal distribution, and the structural function is $Z = \ln(D/D_{LS_i})$, and the probability of exceedance is expressed by

$$P_f = \Phi\left(\frac{\ln\left(\mu_D\right) - \ln\left(\mu_{D_{LS_i}}\right)}{\sqrt{\sigma^2_{\ln D} + \sigma^2_{\ln D_{LS_i}}}}\right), \tag{23}$$

where $\mu_{D_{LS_i}}$ is the mean threshold of story damage factor corresponding to the ith performance level, and $\sigma_{\ln D_{LS_i}}$ is the standard deviation of the threshold for story damage factor of the ith performance level. Note that $\sigma^2_{\ln D_{LS_i}} = 0.399$ [32].

Table 1: The threshold of damage factors of different performance levels.

Damaged condition	NO	IO	LS	CP
Liu [29]	0.10	0.30	0.60	0.85

5. Case Study

5.1. Selection of Seismic Ground Motions. According to the Chinese code for seismic design of buildings [23], 20 seismic ground motions are selected from the database of Pacific Earthquake Engineering Research Center (PEER), as shown in Table 2.

5.2. The Worst-Case Input Angle of Seismic Ground Motion. The worst-case input angle of the seismic ground motion is determined using the proposed method in Section 2. In order to verify the proposed method, three finite element models with different geometric shapes are established, as shown in Figure 4. The fundamental frequency in X-direction of structures A, B, and C is 0.97, 2.63, and 1.81, and in Y-direction, 1.09, 2.03, and 1.96, respectively.

According to Equation (3), the corresponding scale coefficient a can be obtained. Taking the Imperial Valley-06 among the 20 selected seismic ground motions as an example, it is decomposed at input angle equal to 0°, 20°, 40°, 60°, 80°, 100°, 120°, 140°, 160° and 180°, respectively. Then, a and the 'db4' wavelet function are used to perform wavelet transform at X_θ, from which C (a, b) can be obtained. Finally, effective input energy is acquired through computing the area enclosed by C (a, b) and the time axis. The results are shown in Figure 5, in which the X-axis is the input angle of seismic ground motion, and the Y-axis is the effective input energy corresponding to different input angles.

Figures 5(a)–5(c) are the effective input energy in the X-direction of structure A, structure B, and structure C, respectively, in which the X-axis represents the input angle of seismic ground motion, and the Y-axis represents the effective input energy corresponding to different input angles. The Imperial Valley-06 is again taken as an example, with which elastoplastic analysis of the structure is performed at input angle 0°, 20°, 40°, 60°, 80°, 100°, 120°, 140°, 160°, and 180°, respectively. Then, the maximum top displacement of structure is obtained at different input angles. Figures 5(g)–5(i) show the X-direction maximum top displacement of structure A, structure B, and structure C, respectively, in which the X-axis represents the input angle of seismic ground motion, and the Y-axis represents the maximum top displacement of structure corresponding to different input angles.

Accordingly, Figures 5(d)–5(f) are the effective input energy in the Y-direction of structure A, structure B, and structure C, respectively. Figures 5(j)–5(l) are the Y-direction maximum top displacement of structure A, structure B, and structure C, respectively.

For structure A, the tendency that the X-direction effective input energy changes with the input angles can be

Table 2: Information of the selected seismic ground motions.

Number	Magnitude	Time	Earthquake name	PGA	PGV	PGV/PGA	Member
1	6.5	1979	Imperial valley-06	0.439	109.8	0.255	E06230
2	6.5	1987	Superstitn Hills (B)	0.455	112.0	0.251	PTS225
3	6.7	1994	Northridge-01	0.604	78.2	0.132	SYL090
4	6.9	1980	Irpinial, Italy-01	0.358	52.7	0.150	STU270
5	6.9	1989	Loma Prieta	0.324	42.6	0.134	STG090
6	7.0	1992	Cape Mendocino	0.662	89.7	0.138	PET090
7	7.3	1992	Landers	0.721	97.6	0.138	LCN275
8	6.7	1994	Northridge-01	0.838	166.1	0.202	RRS228
9	6.7	1992	Erzican, Turkey	0.515	83.9	0.166	ERZ-NS
10	7.1	1999	Duzce, Turkey	0.535	83.5	0.159	DZC270
11	7.1	1999	Hector Mine	0.306	34.21	0.114	HECTOR/HEC090
12	7.4	1990	Manjil, Iran	0.505	43.78	0.088	MANJIL/ABBAR-T
13	7.1	1999	Duzce, Turkey	0.822	62.1	0.077	DUZCE/BOL090
14	7.5	1999	Kocaeli, Turkey	0.358	46.4	0.132	KOCAELI/DZC090
15	7.5	1999	Kocaeli, Turkey	0.249	29.5	0.121	KOCAELI/ARC090
16	6.9	1995	Kobe, Japan	0.212	27.9	0.134	KOBE/SHI090
17	6.9	1995	Kobe, Japan	0.503	36.6	0.074	KOBE/NIS090
18	6.7	1994	Northridge	0.482	45.1	0.095	NORTHR/LOS270
19	6.7	1994	Northridge	0.516	62.8	0.124	NORTHR/MUL279
20	7.3	1992	Landers	0.417	42.3	0.103	LANDERS/CLW-TR

PGA—Peak Ground Acceleration; PGA—Peak Ground Velocity.

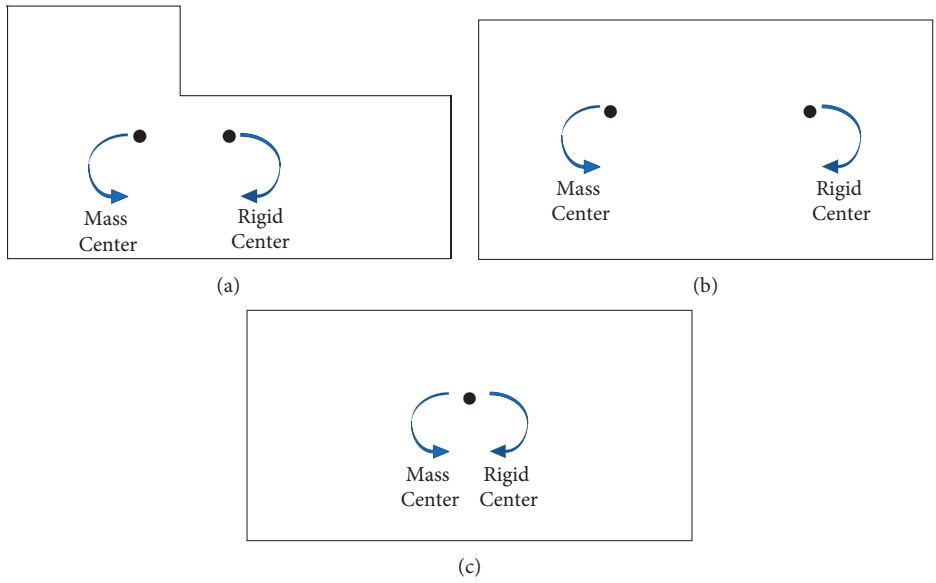

Figure 4: Plan view of structure with different geometric shapes. (a) Plan view of L-shaped structure (Structure A). (b) Plan view of plan-asymmetric rectangle structure (Structures B). (c) Plan view of plan-symmetric rectangle structure (Structure C).

described as "$\wedge$", and the X-direction top displacement changes with the input angles also as "$\wedge$". The X-direction maximum effective input energy is about 545, and the corresponding worst-case input angle is about 105°. The maximum top displacement is 0.053 m, and the corresponding worst-case input angle is also about 105°. The minimum top displacement is 0.020 m, which is 62.3% smaller than the maximum top displacement. When input angle is 0° that is widely used in practice, the top displacement is 0.027 m, which is 49.1% smaller than the top displacement corresponding to input angle 105° (the worst-case input angle).

For structure B, the tendency that the effective input energy in the X-direction changes with the input angles can be expressed as "$\vee$", and the X-direction top displacement changes with the input angles also as "$\vee$". The maximum effective input energy in the X-direction is about 300, and the corresponding worst-case input angle is about 140°. The maximum top displacement is 0.027 m, and the corresponding worst-case input angle is also about 140°, while the minimum top displacement is 0.017 m, which is 37.0% smaller than the maximum top displacement. When input angle is 0°, the top displacement is 0.020 m, which is 25.9% smaller than the maximum top displacement.

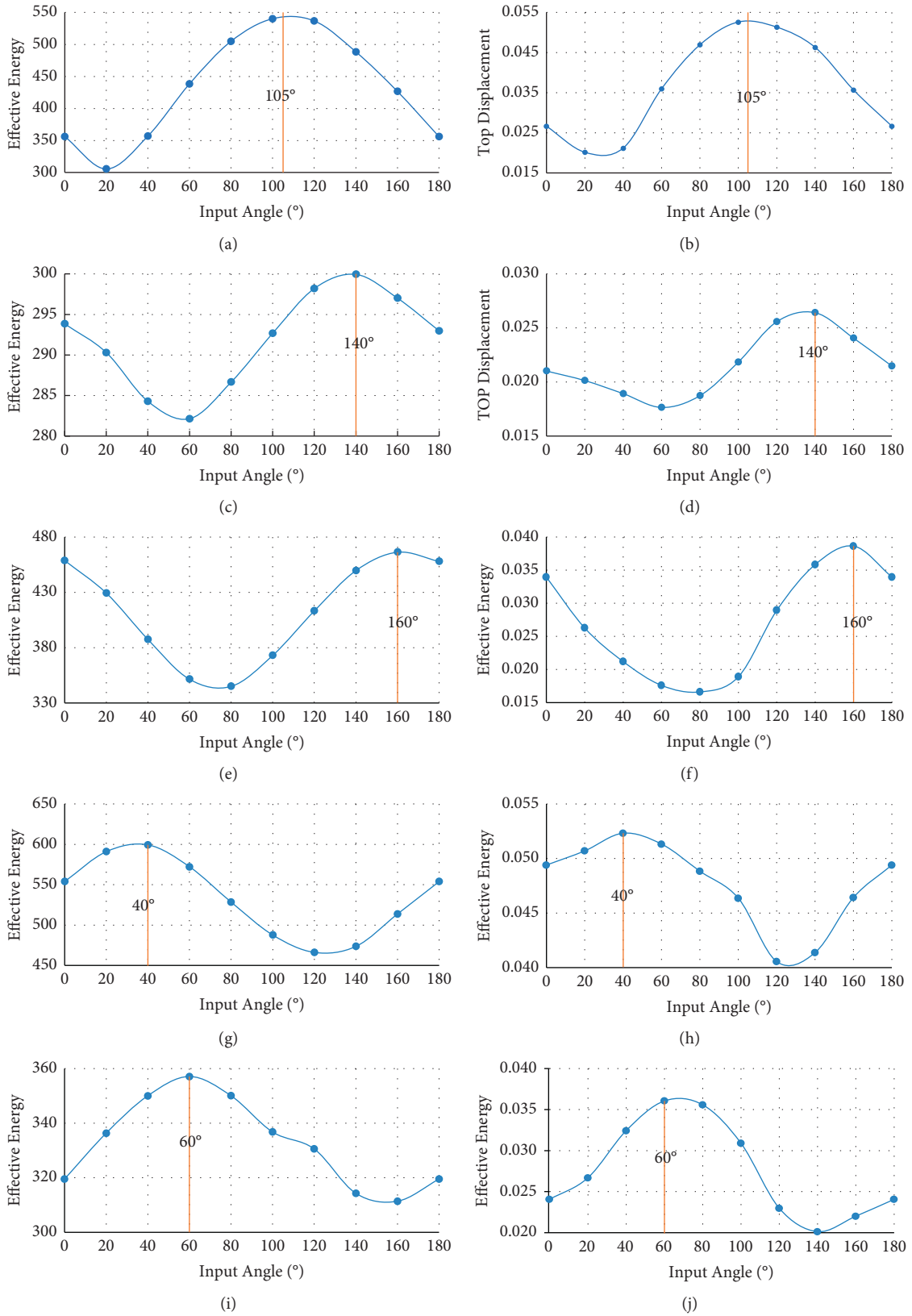

Figure 5: Continued.

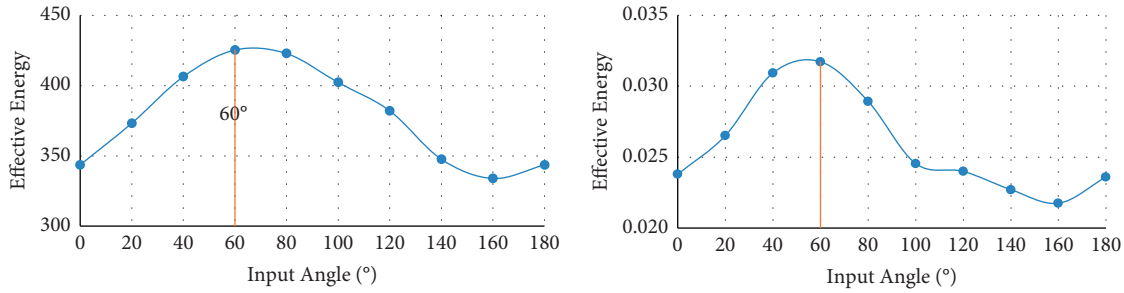

Figure 5: The effective input energy and top displacement of structure A, structure B, and structure C under imperial valley-06 at different input angles. (a) The effective input energy in the X-direction of structure A. (b) The effective input energy in the X-direction of structure B. (c) The effective input energy in the X-direction of structure C. (d) The effective input energy in the Y-direction of structure A. (e) The effective input energy in the Y-direction of structure B. (f) The effective input energy in the Y-direction of structure C. (g) The top displacement in the X-direction of structure A. (h) The top displacement in the X-direction of structure B. (i) The top displacement in the X-direction of structure C. (j) The top displacement in the Y-direction of structure A. (k) The top displacement in the Y-direction of structure B. (l) The top displacement in the Y-direction of structure C.

For structure C, the tendency that the effective input energy in the X-direction changes with the input angles can be expressed as "$\wedge$", and the X-direction top displacement changes with the input angles also as "$\wedge$". The maximum effective input energy in the X-direction is about 466, and the corresponding worst-case input angle is about 160°. The maximum top displacement is 0.038 m, and the corresponding worst-case input angle is also about 160°, while the minimum top displacement is 0.017 m, which is 55.3% smaller than the maximum top displacement. When input angle is 0°, the top displacement is 0.034 m, which is 10.5% smaller than the maximum top displacement.

We can conclude that the seismic response of the structure changes significantly with the variations of the input angle. From the comparison of the selected structures in the article, for structure A, the ratio of the minimum and maximum top displacement changes the most (the minimum top displacement is 62.3% smaller than the maximum top displacement); also, ratio of the maximum top displacement and the top displacement corresponding to input angle 0° is the largest (the top displacement corresponding to input angle 0° is 49.1% smaller than the maximum top displacement). The input angle will obviously affect the seismic response of both plan-symmetric and plan-asymmetric structures. When the input angle is 0°, which is common in conventional structural analysis methods, the seismic response of the structure may be underestimated.

At the same time, it can be seen from the above analysis that, with the change of the input angle, the effective input energy and the top displacement variation trends are basically the same. Both the maximum input energy and the maximum top displacement approximately correspond to input angle 100°, 140°, and 160°, for structures A, B, and C, respectively. In other words, after the seismic ground motion is decomposed according to different angles, the input angle corresponding to the maximum effective input energy can be obtained by wavelet transforms, which also corresponds to the maximum seismic response of the structure; i.e., the input angle is the worst-case input angle of seismic ground motion. In general, the method of using wavelet transforms to find the worst-case input angle of seismic ground motion proposed in this paper is reasonable and accurate. Similar conclusions can be obtained for Y-direction of structures A, B, and C, as shown in Figures 5(d)–5(f), 5(j)–5(l).

5.3. Calculation of the Damage Factor of Structure. In this study, structure A, which is an eight-floor RC plan-asymmetric wall-frame structure, is taken as an example to calculate the damage factor and conduct fragility analysis. In the analysis process, the worst-case input angle of each seismic ground motion is used, and the method for determine the worst-case input angle is referred to in Section 2. II damage model is used to calculate story damage factor as shown in Section 3. Accordingly, the seismic fragility analysis is performed to obtain a set of demand measures, which are evaluated under critical damage states as shown in Section 4.

5.3.1. The Numerical Simulation. In this study, the proposed method is used to evaluate the damage of the structure A. According to the Chinese code for seismic design of buildings [23], the seismic fortification category of the structure is Class B, the seismic fortification intensity is 8 degrees (0.2 g), the earthquake grouping belongs to the third group, and the site category is Class II. The structure plan is shown in Figure 6; specially, the 6 columns marked with a red frame are removed from the eighth floor, so as to meet the functional requirements. The grade of the reinforcement used in the diaphragm, beam, column, and shear-wall is HPB300, HRB335, and HRB400, respectively. The grade of stirrup is HPB235. The mechanical properties of concrete and reinforcement are detailed in the Chinese code for design of concrete structures [33]. The thickness of the shear-wall between axis A and B is 400 mm, and that of the remaining shear-wall is 300 mm. The thickness of the diaphragm is 100 mm, the sectional dimension of the beam is 300 mm (width) and 700 mm (height), and the rest of structural parameters are shown in Table 3.

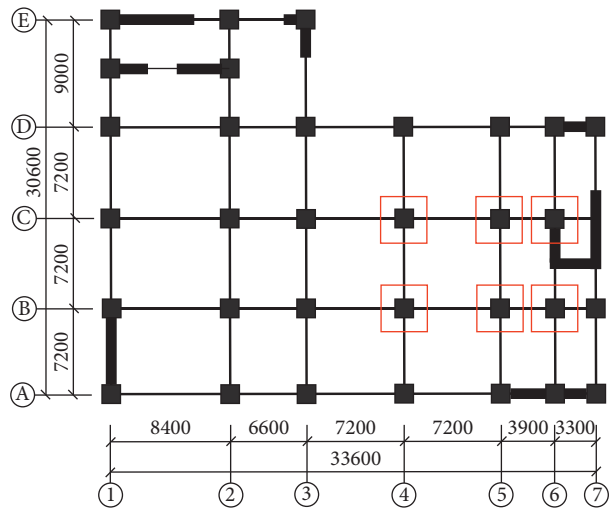

Figure 6: The structural plan of structure A (Unit: mm).

Table 3: Main structural parameters.

Floor	Column section (unit: mm*mm)	Concrete grade of the column	Concrete grade of the beam
1~5	800*800 (Edge column) 700*700 (Middle column)	C40 C40	C30
6~8	800*800 (Edge column) 600*600 (Middle column)	C30 C30	C30

The uniaxial stress-strain relationship in Appendix C.2.4 of Reference [33] is used as the constitutive relationship of unconstrained concrete; for constrained concrete, stress-strain relationship of the axial compressive strength of concrete proposed by Mander et al. is used, in which confinement effect of the stirrup to the concrete is considered [34]. The constitutive relationship of reinforcement adopts the stress-strain relationship of reinforcement with yield point in Appendix C.1.2 of Reference [33].

In Perform-3D, the frame beam and the frame column are simulated with FEMA Beam (Concrete type) and FEMA Column (Concrete type), respectively. FEMA Beam and FEMA Column are used to simulate the nonlinear behavior of the whole structural component rather than only the plastic deformation at both ends. Based on the force-deformation curve in FEMA 356 [35], FEMA 445 [36], and Perform-3D, as shown in Figure 7, combining with the inelastic deformation index in FEMA 356 [35], the threshold value corresponding to certain limit state of structural component can be determined.

The coupling beam can be simulated by either general wall element or beam element. The coupling beam with large span-depth ratio may produce considerable bending deformation, while it suffers shear failure, and for coupling beam suffering bending-shear failure or bending failure, it is more complex to simulate it with wall element in Perform-3D, and the analysis process will also be quite time-consuming. The minimum span-depth ratio of the coupling beam in the case study is 3.6, which is relatively large. Therefore, the coupling beam is simulated as follows: two elastic beam elements + middle shear hinge + bending hinge at both ends of the beam. When the coupling beam is linked with the shear-wall in the plane, the embedded beam element is added in the shear-wall limb to reflect the rigid connection between the coupling beam and the shear-wall. The force-deformation curve of the shear hinge is shown in Figure 8, and the calibration of nonlinear characteristics of coupling beam shear hinge refers to ASCE 41 [37]. In Figure 7, FY is the yield shear and can be obtained according to Equation (24); FR is 0.3 times FY.

$$F_Y = 2A_s\sqrt{f_c'} + f_y A_{sv} d. \tag{24}$$

Based on Figure 7, combined with the shear angle of the component, the damage state of the component can be judged. When the shear angle of the component is 0~0.005, which means that the component is slightly damaged, it corresponds to the damage state of the component that the first diagonal crack appears in the middle of the coupling beam along the diagonal direction, and its direction roughly points to the compression diagonal at both ends of the beam; when the shear angle of the component is 0.005~0.012, the component is in the medium damage stage, which represents the damage state that the diagonal crack zone can be formed near the diagonal of the coupling beam with the increase of the seismic peak ground acceleration; finally, when the shear angle of the component is greater than 0.016, the concrete in the middle of the coupling beam is crushed, resulting in a significant decrease in the bearing capacity of the component and even the failure of the whole component.

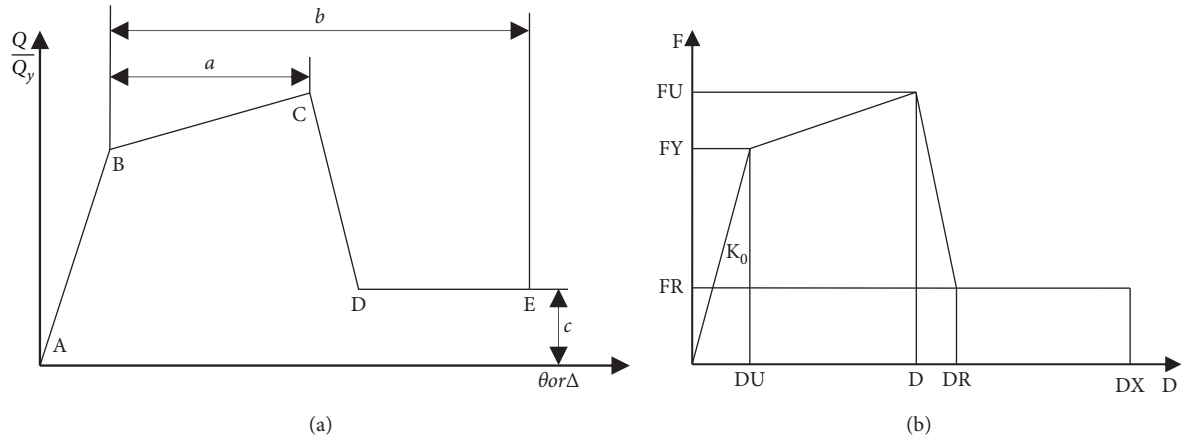

Figure 7: Force-deformation curve of the component in FEMA 356 and Perform-3D. (a) FAME 356. (b) Perform-3D.

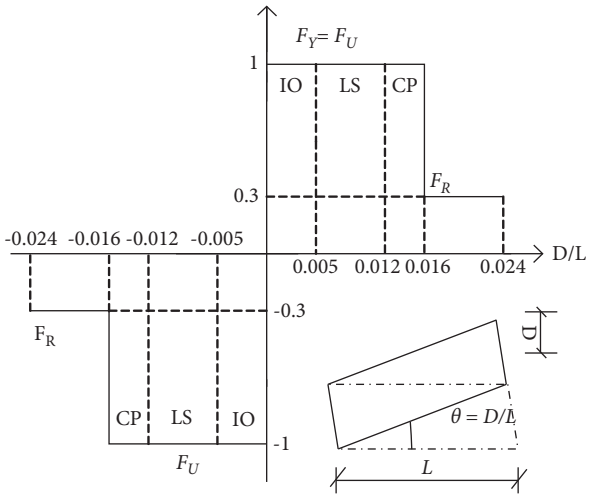

Figure 8: Force-Deformation curve of the component in FEMA 356 and Perform-3D.

The shear-wall is simulated multilayer shell element. The web shear-wall is composed of unconstrained concrete layer and reinforcement layer, while flange wall is divided into two types: one is composed of reinforcement layer and concrete layer, and that of the other is reinforcement layer and confined boundary element.

5.3.2. The Importance Coefficients of Structural Components. The importance coefficient of the structural component is calculated using the method in Section 3.3. The generalized stiffness of component i after its failure and that of the original structure are obtained through Equation (14), the importance coefficient of component i is acquired through Equation (15), and the results are shown in Figure 9. The importance coefficient of the frame beam in the first story is 0.004. The importance coefficients of columns A and B are 0.014 and 0.015, respectively. The importance coefficient of the shear-wall marked with red circle is 0.132. The importance coefficient of shear-wall is the largest in each story, while that of beam is the smallest. Moreover, the maximum importance coefficient occurred on the first story. Meanwhile, the importance coefficient decreases with the increase of structural height. The distribution of the importance coefficient is in accordance with the damage degree of the component in seismic damage structures. Hence, the proposed method can relatively exactly determine the importance coefficients of structural components properly.

5.3.3. Distribution of the Hysteresis Energy Dissipation. The hysteretic energy dissipation of structures would occur at critical structural components [38]. Hence, the key components should be designed carefully to ensure their hysteretic energy dissipation ability. Meanwhile, it is meaningful to evaluate the structural damage according to the energy dissipation pattern. Adjusting PGA of 20 selected seismic ground motions to the levels of 0.2 g, 0.4 g, and 0.6 g, the average hysteretic energy dissipation of each component is determined under those seismic ground motions with different levels of PGA. The total hysteretic energy dissipation of the shear-wall on the first floor can be obtained by accumulating the hysteretic energy dissipation of each shear-wall on the first floor, so does that of the coupling beam and frame beam on the first floor. The total hysteretic energy dissipation of the shear-wall, the coupling beam, and the frame beam on each floor is shown in Figure 10. As the hysteretic energy dissipation of the column is relatively small and negligible, it is not shown in Figure 10. For the method of determining hysteretic dissipation, refer to literature [38].

The hysteretic energy dissipation of all structural components significantly increases with the augment of the PGA, as shown in Figures 10(a)–10(c). For example, the hysteretic energy dissipation of the shear-wall at the first story corresponding to PGA levels of 0.2 g, 0.4 g, and 0.6 g is 2.3 kN·m, 113.5 kN·m, and 512.7 kN·m, respectively. Note that the ratio of the hysteretic energy dissipation of the beam on the eighth story to that on the seventh story increases with the augment of PGA, which exceeds one when PGA reaches 0.4 g. The reason for the phenomenon is that the deformation of the structure increases with the increase of PGA. However, on the eighth story, six middle columns are removed, which lengthens the force transfer path of the beam and would produce significant deformation. As a

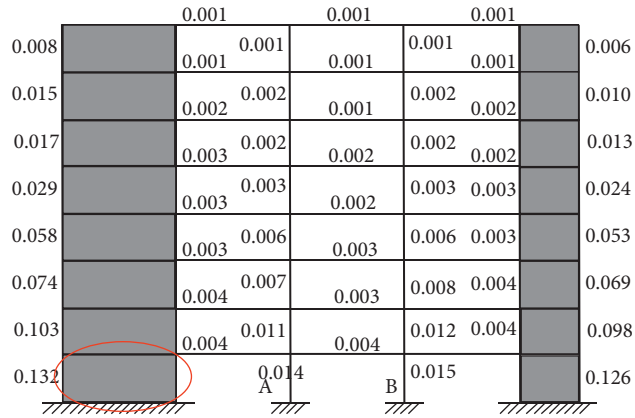

Figure 9: The distribution of importance coefficients of different structural component.

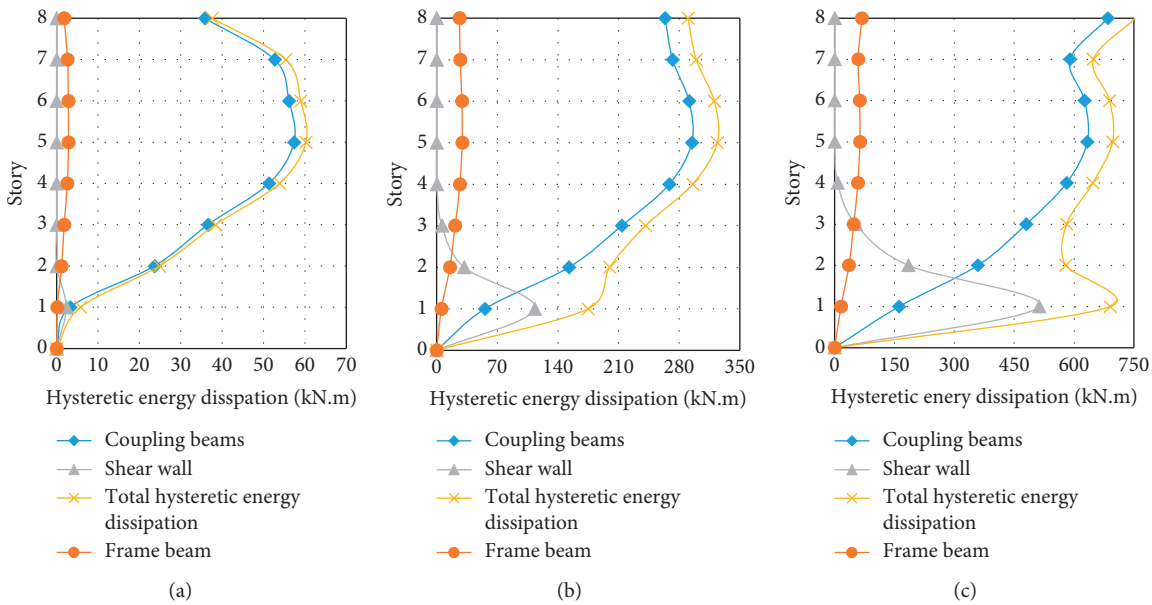

Figure 10: The hysteretic energy dissipation of structure A. (a) PGA = 0.2 g. (b) PGA = 0.4 g. (c) PGA = 0.6 g.

result, irreparable damage would firstly occur in the eighth story when PGA reaches a certain value.

5.3.4. Damage Factor of the Story. The damage factors of all stories are calculated using the method presented in Section 3.4. Adjust PGA of 20 aforementioned seismic ground motions to the levels of 0.2 g, 0.4 g, and 0.6 g. Under these seismic ground motions with different levels of PGA, the average deformation of each component is calculated, the damage factor of each component is obtained through Equations (4)–(7), and the damage factor of the story is obtained through Equations (16)–(20), as shown in Figure 11.

As shown in Figure 11, the damage factor caused by hysteretic energy dissipation is greater than that caused by the deformation at the first story for PGA levels of 0.4 g and 0.6 g, while the opposite is true for 0.2 g. Meanwhile, the damage factor caused by the deformation is greater than that caused by the hysteretic energy dissipation from the second story to the eighth story. The hysteretic energy dissipation of the shear wall mainly occurs on the bottom story, especially the first story. Meanwhile, the deformation of the first story is smaller than the other stories. Hence, damage of the first story caused by hysteretic energy dissipation is greater than that caused by deformation. Note that the damage factors of all stories significantly increase with the augment of PGA. The ratio of the damage produced by hysteretic energy dissipation to the total damage increases with the augment of PGA. For example, the ratio of the seventh story is 13%, 20%, and 26% corresponding to PGA levels of 0.2 g, 0.4 g, and 0.6 g, respectively.

5.3.5. Comparison of Damage Factors. Based on the results of Figure 10, the story damage factors calculated using Equation (3) are termed as results of II model, and when Equation (4) is used, that can be termed as results of Du model. The comparison between the results of II model and

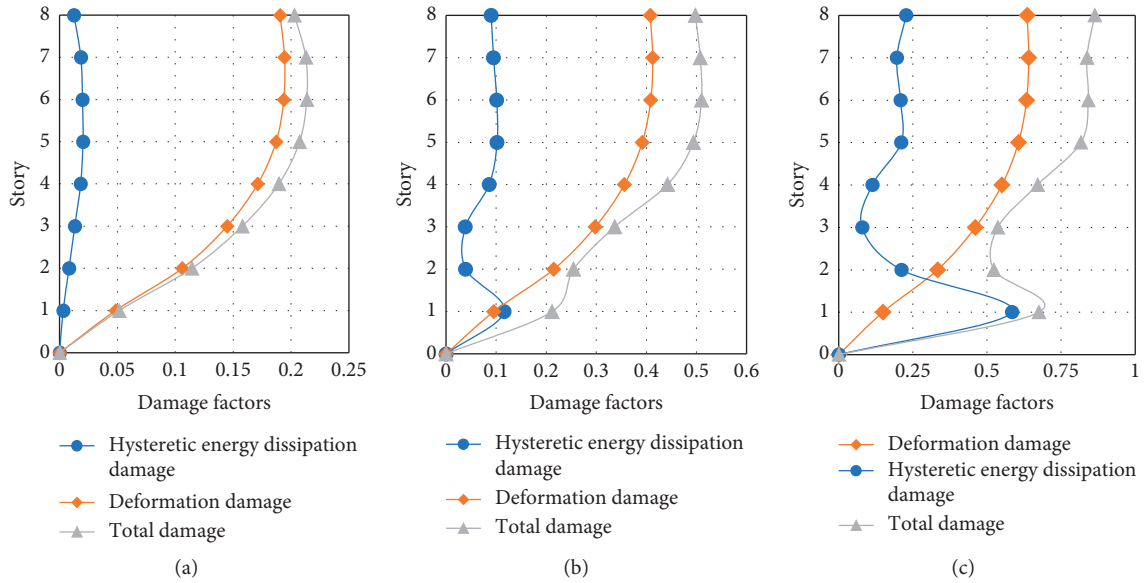

Figure 11: The damage factors of stories. (a) PGA = 0.2 g. (b) PGA = 0.4 g. (c) PGA = 0.6 g.

Table 4: Comparison of damage factors on the first story.

PGA	Shear-wall damage factor (Du damage model)	Story damage factor (Du damage model)	Story damage factor (II damage model)
0.2	0.05	0.04	0.049
0.4	0.21	0.19	0.205
0.6	0.67	0.59	0.667

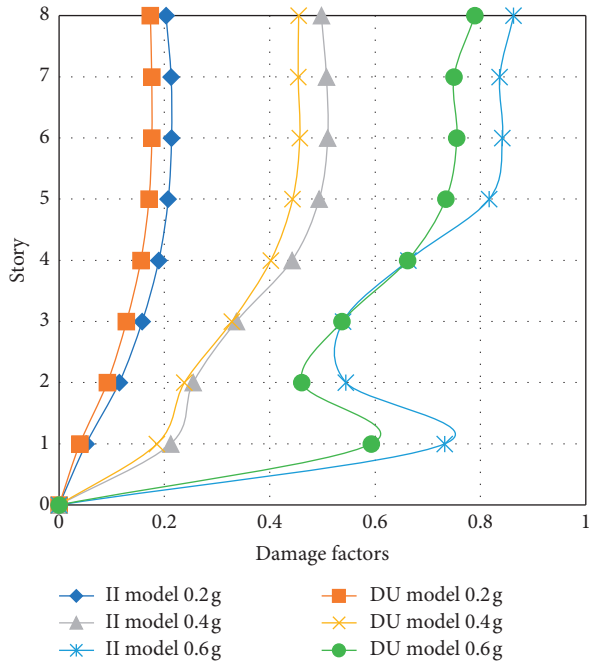

Figure 12: Comparison of damage factors.

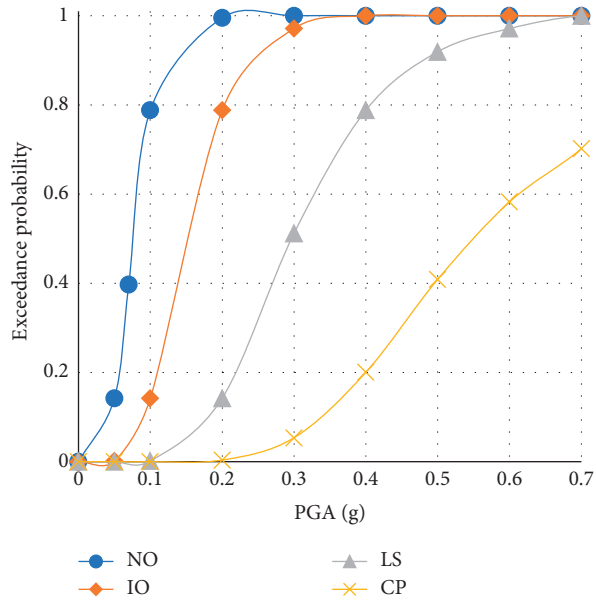

Figure 13: The fragility curves.

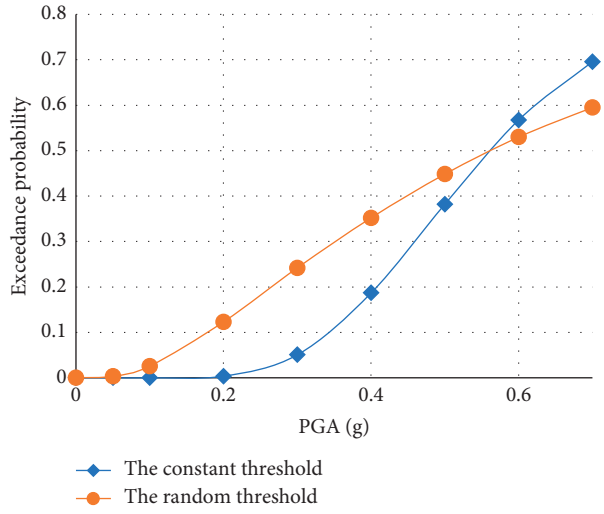

Figure 14: The fragility curves corresponding to CP limit state.

Du model on the first story is shown in Table 4, and that for each story is shown in Figure 12.

As shown in Table 4, based on Du damage model, the damage factor of shear-wall on the first story is 0.67, and the story damage factor of the first story is 0.59. The damage factor of shear-wall is significantly greater than the story damage factor of the first story if Du damage model is used. However, the damage of the first story is mainly induced by the damage of the shear-wall, which is concluded from the seismic damage investigation [39]. The conflict is produced by the reason that the importance coefficients of structural components are ignored in Du damage model. Hence, the damage of the first story may be underestimated under Du damage model, while the damage factor of the shear-wall is close to the story damage factor of the first story based on II damage model.

From Figure 12, the story damage factor calculated using II damage model is greater than that using Du damage model. As importance coefficients of structural components are taken into account in the damage factor corresponding to II damage model, the hysteretic energy dissipation of the shear-wall is highly weighted for the lower story. Meanwhile, the deformation of columns is highly weighted for the middle and upper story. Hence, it is reliable that the damage is evaluated using II damage model.

5.3.6. Fragility Analysis. Based on Section 3.4, the maximum story damage factor is taken as the global damage factor of the structure. The global damage factor corresponding to different seismic ground motions and the threshold of the damage factors for different damage states

Table 5: Variables involved in the paper.

Symbol	Explanation
$C(a,b)$	Wavelet transforms coefficient
a	Scale coefficient
b	Position coefficient
$\varphi(a,b,t)$	Wavelet function
$E(a,b)$	Wavelet energy
F_a	The frequency of the structure
F_c	The center frequency of the wavelet
Δ	The sampling interval
D_{if}	The damage factor of component i on the f^{th} story
D_{bif}	The damage factor of component i caused by deformation of the f^{th} story
D_{hif}	The damage factor of component i caused by energy dissipation of the f^{th} floor;
δ_m	The maximum displacement of component under earthquake action
δ_u	The ultimate displacement of component under monotonic load
Q_y	The yield strength of the component
$\int \mathrm{d}\varepsilon$	The total hysteretic energy dissipation of the component
λ	The shear span ratio
λ_N	The axial compression ratio
ρ	The longitudinal reinforcement ratio
ρ_ω	The volumetric stirrup ratio
D_f	The damage factor of the f^{th} story
λ_{if}	The weighted combination coefficient of component i in the f^{th} story
E_{if}	The hysteretic energy dissipation of component i in the f^{th} story
U	The strain energy of the initial structure
$\{D\}$	The displacement vector of the structure
$\{F\}^T$	The load vector of the structure
F_S	The generalized force
D_S	The generalized displacement
I_i	The loss rate of the generalized stiffness
$K_{N,0}$	Generalized stiffness of the initial structure
$K_{N,i}$	The generalized stiffness of the residual structure after the failure of component i
D_{bf}	The damage factors of f^{th} story caused by the deformation
D_{hf}	The damage factors of f^{th} story caused by the hysteretic energy dissipation
λ_{bif}	The weighted combination coefficients of component i on f^{th} story corresponding to deformation
λ_{hif}	The weighted combination coefficients of component i on f^{th} story corresponding to hysteretic energy dissipation
I_{if}	The importance coefficient of component i on f^{th} story
D	The maximum story damage factor
D_{LS_i}	The threshold for story damage factor of the ith performance level
$\Phi(\cdot)$	The standard normal probability distribution
μ_D	The mean value of the maximum story damage factor
σ_{lnD}	The standard deviation of the maximum story damage factor

(or performance levels, refer to Table 1) are brought into Equation (21) to obtain the exceedance probability of different damage states, as shown in Figure 13. The threshold of the damage factor, which equals 0.85 (i.e. corresponding to collapse of the structure), together with the global damage factor corresponding to different seismic ground motions is brought into Equation (22) to acquire the exceedance probability with a fixed threshold value, and if they are brought into Equation (23), the exceedance probability with random threshold values will be obtained, as shown in Figure 13. Note that the damage factors represent the performance indexes. Figure 13 shows the fragility curves developed for different performance levels (NO, IO, LF, and CP) and associated with the different damage measures under 20 aforementioned ground motions.

As shown in Figure 13, the fragility curve corresponding to NO limit state is steeper than that of the other performance levels, while the probability of exceedance for the CP limit state is the smallest. The probabilities of exceedance for all performance levels increase with the augment of PGA. The probability exceeds 0.723, when PGA reaches to 0.7 g corresponding to CP limit state.

The fragility curves of CP limit state with constant threshold and random threshold are shown in Figure 14. The probability of exceedance with constant threshold is less than that with random threshold when PGA ranges from 0 to 0.53 g. The opposite is true, when PGA ranges from 0.53 g to 0.7 g. Hence, the randomness of the threshold significantly affects the fragility of structures.

6. Conclusions

In this study, the worst-case input angle of the bidirectional earthquake excitation is identified using the wavelet transforms coefficient method. The enhanced damage model is

used to identify the floor damage factors, which takes into account the importance coefficients of structural components. Meanwhile, the classic probabilistic seismic fragility assessment method is used to assess the performance of RC plan-asymmetric wall-frame structures based on the enhanced damage model. Moreover, the randomness of the threshold value is used during the seismic fragility assessment of RC plan-asymmetric wall-frame structures. The following conclusions can be drawn from this study:

(1) The importance coefficient, which measures the contribution of different structural components to the global resistance of the whole story or structure, is introduced to the evaluation of floor damage. For RC wall-frame structures, especially on the lower floors, the damage factor increases obviously than that of Du model, and the rate of increase of damage factor is more significant with the increase of PGA.

(2) From the comparison of the damage factors corresponding to the deformation and hysteretic energy dissipation of each floor, for middle and upper floors, it can be seen that the damage caused by deformation is significantly severer than that caused by energy dissipation; however, for the lower floor, the opposite is true. Based on this, this type of structure can be treated pertinently in engineering seismic design and seismic retrofit.

(3) As the introduction of the importance coefficient of the component, by which the importance of vertical component is emphasized, the story damage factor determined with II model is greater than that determined with Du model. For lower floors, the energy dissipation of vertical component (i.e., shear-wall) contributes much more to the story damage than the deformation of that; for middle and upper floors, the contribution of the deformation of shear-wall is more significant, which makes the global damage factor larger than that of Du model; in other words, the results of damage evaluation are more safe and reliable.

(4) When $0 < \mathrm{PGA} < 0.53$ g, the exceedance probability with constant threshold is less than that with random threshold; when $0.53\ \mathrm{g} < \mathrm{PGA} < 0.7$ g, the opposite is true. Therefore, the randomness of the threshold has a significant impact on the fragility of the structure.

All symbols of variables used in this article are shown in Table 5.

Data Availability

All the data, models, or code generated or used during the study are available from the corresponding author upon request.

Conflicts of Interest

The authors declare that there are no conflicts of interests regarding the publication of this paper.

Acknowledgments

This paper was supported by the Qinghai Natural Science Foundation under Grant (grant number 2018-ZJ-938Q) and the Qinghai Innovation Platform Construction Special Project (grant number 2018-ZJ-T01).

References

[1] F. Sharmin, M. Hussan, and D. Kim, "Influence of soil-structure interaction on seismic responses of offshore wind turbine considering earthquake incident angle," *Earthquakes and Structures*, vol. 13, no. 1, pp. 39–50, 2017.

[2] H. P. Hong and S. C. Yang, "Reliability and fragility assessment of the mid- and high-rise wood buildings subjected to bidirectional seismic excitation," *Engineering Structures*, vol. 201, Article ID 109734, 2019.

[3] D. S. Zhu, S. Z. Liu, and L. S. Yu, "Research on seismic response of curved girder bridges," *China Journal of Highway and Transport*, vol. 15, no. 3, pp. 42–48, 2002, in Chinese.

[4] D. S. Zhu, L. S. Yu, and S. Z. Liu, "The study of earthquake input principal direction for irregular bridges," *Journal of Lanzhou Railway University*, vol. 19, no. 6, pp. 37–40, 2000, in Chinese.

[5] Y. Ni, J. Chen, H. Teng, and H. Jiang, "Influence of earthquake input angle on seismic response of curved girder bridge," *Journal of Traffic and Transportation Engineering*, vol. 2, no. 4, pp. 233–241, 2015.

[6] N. D. Lagaros, "Multicomponent incremental dynamic analysis considering variable incident angle," *Structure and Infrastructure Engineering*, vol. 6, no. 1-2, pp. 77–94, 2010.

[7] R. Mojtaba and H. Ali, "Structural damage identification through sensitivity-based finite element model updating and wavelet packet transform component energy," *Structure*, vol. 33, pp. 4857–4870, 2021.

[8] R. Sharbati, H. R. Ramazi, F. Khoshnoudian, H. R. Amindavar, and H. Rabbani, "Stochastic model for simulation of ground-motion sequences using kernel-based smoothed wavelet transform and Gaussian mixture distribution," *Journal of Earthquake Engineering*, vol. 25, no. 11, pp. 2147–2177, 2021.

[9] X. Y. He and H. N. Li, "Application of wavelet transform in muti-components seismic response of offshore platform," *Journal of Vibration and Shock*, vol. 26, no. 12, pp. 49–54, 2000, in Chinese.

[10] B. R. Ellingwood, "Earthquake risk assessment of building structures," *Reliability Engineering & System Safety*, vol. 74, no. 3, pp. 251–262, 2001.

[11] K. Porter, R. Kennedy, and R. Bachman, "Creating fragility functions for performance-based earthquake engineering," *Earthquake Spectra*, vol. 23, no. 2, pp. 471–489, 2007.

[12] Y. Li, R. Song, and J. W. Van De Lindt, "Collapse fragility of steel structures subjected to earthquake mainshock-aftershock sequences," *Journal of Structural Engineering*, vol. 140, no. 12, Article ID 04014095, 2014.

[13] J. Park, P. Towashiraporn, J. I. Craig, and B. J. Goodno, "Seismic fragility analysis of low-rise unreinforced masonry structures," *Engineering Structures*, vol. 31, no. 1, pp. 125–137, 2008.

[14] H. Tajammolian, F. Khoshnoudian, A. Rezaei Rad, and V. Loghman, "Seismic fragility assessment of asymmetric structures supported on TCFP bearings subjected to near-field earthquakes," *Structure*, vol. 13, pp. 66–78, 2018.

[15] M. Bhandari, S. D. Bharti, M. K. Shrimali, and T. K. Datta, "Seismic fragility analysis of base-isolated building frames excited by near- and far-field earthquakes," *Journal of Performance of Constructed Facilities*, vol. 33, no. 3, Article ID 04019029, 2019.

[16] B. J. Yin, S. M. Huang, Y. T. Xue et al., "Seismic damage investigation and thinking on the damage buildings of frame-shear wall structure in Wenchuan 5.12 earthquake," *Earthquake resistant engineering and Retrofitting*, vol. 30, no. 4, pp. 37–40, 2008, in Chinese.

[17] T. N. Do and F. C. Filippou, "A damage model for structures with degrading response," *Earthquake Engineering & Structural Dynamics*, vol. 47, no. 2, pp. 311–332, 2017.

[18] T. H. Kim, K. M. Lee, Y. S. Chung, and H. M. Shin, "Seismic damage assessment of reinforced concrete bridge columns," *Engineering Structures*, vol. 27, no. 4, pp. 576–592, 2015.

[19] L. Martins, V. Silva, M. Marques, H. Crowley, and R. Delgado, "Development and assessment of damage-to-loss models for moment-frame reinforced concrete buildings," *Earthquake Engineering & Structural Dynamics*, vol. 45, no. 5, pp. 797–817, 2015.

[20] Y. J. Park, A. H.-S. Ang, and Y. K. Wen, "Seismic damage analysis of reinforced concrete buildings," *Journal of Structural Engineering*, vol. 111, no. 4, pp. 740–757, 1985.

[21] Y. J. Park and H.-S. Alfredo Ang, "Mechanistic seismic damage model for reinforced concrete," *Journal of Structural Engineering*, vol. 111, no. 4, pp. 722–739, 1985.

[22] X. L. Du and J. P. Ou, "Seismic damage evaluation model of building structures," *World Earthquake Engineering*, vol. 7, no. 3, pp. 52–58, 1991, in Chinese.

[23] Gb 50011-2010, *Code for Seismic Design of Buildings*, China Architecture & Building Press, Beijing, China, 2016.

[24] X. C. Lin and L. P. Ye, "Study on optimization of seismic design for RC frames based on member importance index," *Journal of Building Structures*, vol. 33, no. 6, pp. 16–21, 2012, in Chinese.

[25] P. Zhang, S. Hou, and J. Ou, "A beam-column joint element for analysis of reinforced concrete frame structures," *Engineering Structures*, vol. 118, pp. 125–136, 2016.

[26] S. Xiao, L. Xu, and X. Lu, "Nonlinear damage model for seismic damage assessment of reinforced concrete frame members and structures," *Acta Mechanica Sinica*, vol. 34, no. 5, pp. 949–962, 2018.

[27] M. Shokrabadi, M. Banazadeh, M. Shokrabadi, and A. Mellati, "Assessment of seismic risks in code conforming reinforced concrete frames," *Engineering Structures*, vol. 98, pp. 14–28, 2015.

[28] M. E. Rodriguez and D. Padilla, "A damage index for the seismic analysis of reinforced concrete members," *Journal of Earthquake Engineering*, vol. 13, no. 3, pp. 364–383, 2009.

[29] B. Q. Liu, S. L. Bai, and M. Liu, "Equivalent ductility damage criteria of earthquake resistant structures and their verification by substructure method and their verification by substructure method," *Earthquake Engineering and Engineering Viberation*, vol. 17, no. 3, pp. 77–83, 1997.

[30] R. P. Kennedy, C. A. Cornell, R. D. Campbell, S. Kaplan, and H. F. Perla, "Probabilistic seismic safety study of an existing nuclear power plant," *Nuclear Engineering and Design*, vol. 59, no. 2, pp. 315–338, 1980.

[31] X. N. Huang, Y. F. Du, and H. Li, "Multidimensional performance limit states for fragility analyze of plane irregular structure," *Journal of Vibration, Measurement & Diagnosis*, vol. 37, no. 3, pp. 560–566, 2017, in Chinese.

[32] G. Li and G. D. Cheng, *Performance-based Seismic Design*, pp. 198–223, Science press, Beijing, China, 2004.

[33] China Architecture Industry Press, *Gb50011—2010. Code for Design of concrete Structure*, China Architecture Industry Press, Beijing, China, 2015, in Chinese.

[34] J. B. Mander, M. J. N. Priestley, and R. Park, "Theoretical stress-strain model for confined concrete," *Journal of Structural Engineering*, vol. 114, no. 8, pp. 1804–1826, 1988.

[35] Federal Emergency Management Agency (Fema), *FEMA 356: Commentary on the Guidelines for the Seismic Rehabilitation of Buildings*, pp. 211–276, American Society of Civil Engineers, Washington, DC, USA, 2000.

[36] Federal Emergency Management Agency (Fema), *FEMA 445: Next-Generation Performance-Based Seismic Design Guidelines*, American Society of Civil Engineers, Washington, DC, USA, 2006.

[37] American Society of Civil Engineers, *Asce41-06. Seismic Rehabilitation of Existing Buildings*, American Society of Civil Engineers, Washington, DC, USA, 2007.

[38] Z. W. Miao, L. P. Ye, Z. Y. Qiu, and A. K. Li, "Distribution mode of hysteretic energy and damage mechanism of RC frame-shear-wall structure under strong earthquakes," *Journal of Southeast University (Natural Science Edition)*, vol. 42, no. 5, pp. 933–939, 2012, in Chinese.

[39] B. Sun and G. Zhang, "The Wenchuan earthquake creation of a rich database of building performance," *Science China Technological Sciences*, vol. 53, no. 10, pp. 2668–2680, 2010.